Volume 7 | Number 2 | 14 January 2015 | Pages 369–844

Nanoscale

www.rsc.org/nanoscale

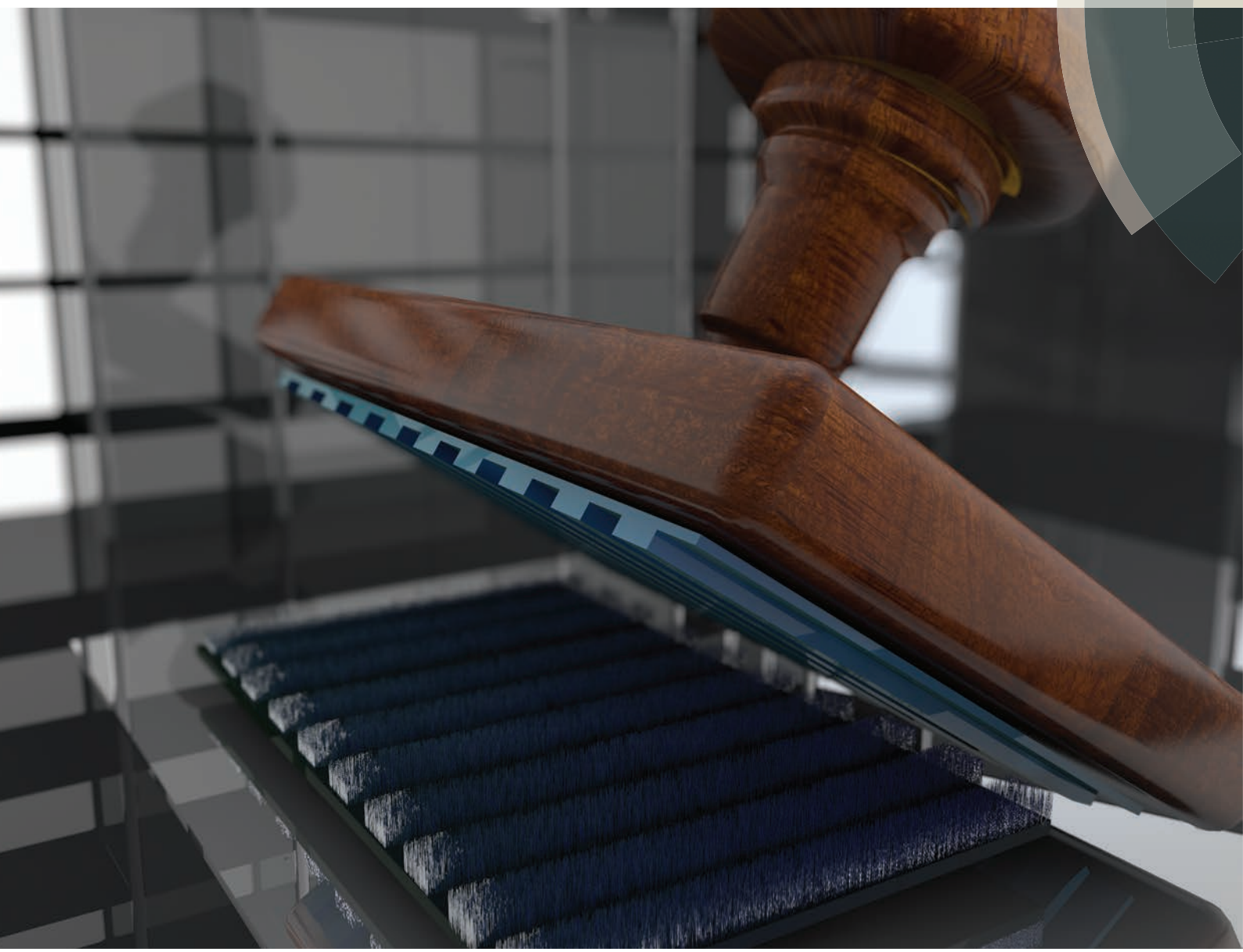

ISSN 2040-3364

ROYAL SOCIETY OF CHEMISTRY

REVIEW ARTICLE
K. Swaminathan Iyer, Igor Luzinov *et al.*
Capillary force lithography: the versatility of this facile approach in developing nanoscale applications

NCNST

Nanoscale

REVIEW

View Article Online
View Journal | View Issue

Cite this: *Nanoscale*, 2015, **7**, 401

Capillary force lithography: the versatility of this facile approach in developing nanoscale applications

Dominic Ho,†[a,b] Jianli Zou,†[c] Bogdan Zdyrko,[d] K. Swaminathan Iyer*[a] and Igor Luzinov*[d]

Received 26th June 2014,
Accepted 11th September 2014

DOI: 10.1039/c4nr03565h

www.rsc.org/nanoscale

Since its inception as a simple, low cost alternative to more complicated lithographic techniques such as electron-beam and dip-pen lithography, capillary force lithography (CFL) has developed into a versatile tool to form sub-100 nm patterns. Utilizing the concept of a polymer melt, structures and devices generated by the technique have been used in applications varying from surfaces regulating cell growth to gas sensing. In this review, we discuss various CFL methodologies which have evolved, their application in both biological and non-biological research, and finally a brief outlook in areas of research where CFL is destined to make an enormous impact in the near future.

1. Introduction

Recently, there has been much interest in developing miniaturised biosensors, biochips, information storage devices and optical devices in a cost friendly and scalable manner. Photolithography and optical lithography have been and are expected to be the mainstay in fabricating such devices. However, there has been much concern about the limitations the techniques have in fabricating sub-100 nm large area features. These limitations have driven the development of new patterning techniques such as capillary force lithography,[1] electron beam lithography,[2] ion beam lithography,[3] dip pen lithography,[4] secondary sputtering lithography,[5] edge lithography,[6] block copolymer lithography,[7,8] and more recently multiplexed beam pen lithography.[9] Though sub-100 nm features are attainable *via* these techniques, their cost, need for specialised equipment and low throughput in most instances have discouraged their use in industry.

As first reported by Suh *et al.* in 2001,[1] CFL combines the essential feature of nanoimprint lithography (the moulding of a polymer melt) with that of soft lithography (the use of an elastomeric mould). This combination retains the stringent pattern fidelity requirements nanoimprint lithography has over microcontact lithography while negating the need for high pressures needed in nanoimprint lithography. Furthermore, this technique eliminates the need for etching steps to remove any residual resist. CFL has the same working principle as "micro-moulding in capillaries (MIMIC)", a technique which utilizes liquid prepolymers and masks with open ends.[10] However, the distinct advantage of CFL is that it is not affected by the limitation of slow capillary filling rates observed in MIMIC but by the size of the mould applied, making it an attractive technique in fabricating large area patterns.

The development of this technique in recent years has resulted in the fabrication of complicated polymer structures. A dual-scale structure can be easily fabricated by two-step UV-assisted CFL while patterned binary polymer brushes can be generated by CFL, in combination with surface-initiated polymerization.[11,12] Furthermore, well-defined structures generated by CFL have been applied as confinements for virus and cells.[13,14] Finally, the versatility of CFL was demonstrated by the patterning of nanoparticles, leading to potential applications in gas sensing.[15] The goal of this review is to provide the reader a comprehensive outlook regarding the fundamental concepts of capillary force lithography pattern transfer techniques, and the versatility of this technique's applicability in developing various nanoscale applications.

2. Key concepts underlying CFL

Typically, silicon wafers (100) are used as substrates; however, other kinds of organic and inorganic substrates can be used if

[a]*School of Chemistry and Biochemistry, The University of Western Australia, Crawley, WA 6009, Perth, Australia. E-mail: swaminatha.iyer@uwa.edu.au*
[b]*School of Anatomy, Physiology and Human Anatomy, The University of Western Australia, Crawley, WA 6009, Perth, Australia*
[c]*Institute for Integrated Cell-Material Sciences (iCeMS), iCeMS Complex 2, Kyoto University, Yoshida-Honmachi, Sakyo-ku, Kyoto, 606-8501, Japan*
[d]*Department of Materials Science and Engineering, Clemson University, 161 Sirrine Hall, Clemson, South Carolina 29634-0971, USA. E-mail: luzinov@clemson.edu*
† These authors contributed equally to the review.

the surface of interest is planar enough to allow conformal contact with the mould.

2.1. General procedure

When a liquid wets a capillary tube and lowers its free energy, the liquid rises in the capillary tube. CFL utilizes this phenomenon, giving rise to the concept of a polymer melt. A schematic of the basic CFL technique is shown in Fig. 1. First, a polymer layer of glass transition temperature, T_g, is spin-coated onto a substrate. An elastomeric mould *e.g.* PDMS is placed on the polymer layer and heated above T_g to allow the polymer melt to fill up the void space, a process driven by the capillary force. This is important as polymer chains become mobile above their T_g.[16] Following this, the mould can be removed and after cooling to ambient temperature, a negative replica of the mask pattern is transferred onto the substrate.

2.2. Aspect ratio of the mould and patterned structure

The height h of a liquid rising in a tube by the capillary force is given as:[1]

$$h = \frac{2\gamma \cos\theta}{\rho G r}$$

This equation is used to estimate the height of a polymer melt in the mould where γ is the polymer/air surface tension, θ is the contact angle at the polymer–mould interface, ρ is the density of the polymer, G is the gravitational constant, and r is the width of the void in the mould. In the case of polystyrene as an example, γ = 40.7 mN m^{-1}, at 20 °C and ρ = 0.97 g mL^{-1}.

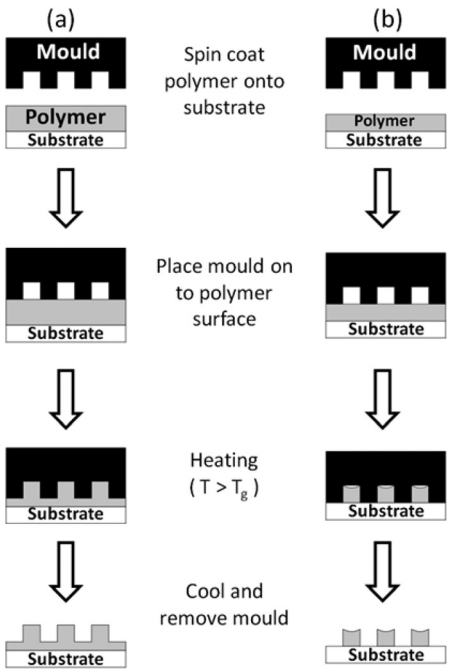

Fig. 1 A schematic representation of CFL. The effect of polymer film thickness on the final pattern. (a) Thick and (b) thin polymer films.

The height of the polymer rising in the mould will be

$$h = \frac{8.6 \times 10^{-6} \cos\theta}{r} m$$

For example, if r = 1 μm and θ = 85°, the polystyrene melt can rise to a maximum height of 0.75 micrometers. As the increase in the polymer melt height is driven by the capillary forces, fabricating high aspect ratio patterns is easily achievable. This concept was further tested experimentally by Suh *et al.*[17] who were able to fabricate structures with step heights as high as 5 μm for an 80 μm line-and-space pattern. Hence, patterning small features with high aspect ratios *via* CFL is largely dependent on the availability of the appropriate moulds and the thickness of the film of interest. As PDMS has very high viscosity, completely filling up the cavity of the high-aspect-ratio mother mould can sometimes be difficult. Furthermore, the deformation of the PDMS mould imposes a resolution limit. The use of a hard fluoropolymer mould can solve this deformation problem and increase the resulting resolution if assisted by high pressure during the CFL process. In addition, polyurethane acrylate moulds, which are stiff enough to replicate dense, sub-100 nm features, have also been used in CFL.[18]

2.3. Thickness of polymer films

As illustrated in Fig. 1, the thickness of the preformed polymer film plays a pivotal role in defining the pattern. When the polymer film is thick enough to completely fill the cavity of the mould, the residual polymer will remain on the substrate. However, if the polymer film is thin and the interaction between the polymer and the substrate is sufficiently weak, no residual film remains and the substrate surface is exposed. In the latter case, a meniscus is observed at the protruding end of the polymer as shown in Fig. 1b; if combined with a "moulded dewetting" process,[19] further annealing could allow the meniscus film to fully dewet from the centre of the meniscus which forms the thinnest part of the film (Fig. 2). Under optimum conditions, the polymer is attracted to the walls of the protruding section of the mould and the resulting feature sizes are much smaller than those of the mould but still inherit the structural characteristics of the mould.

In instances where the polymer film being patterned is sufficiently thin, the meniscus breaks into two, as illustrated in Fig. 3.[20,21] The obtained pattern shows a periodical double structure from the mould used, demonstrating an alternative

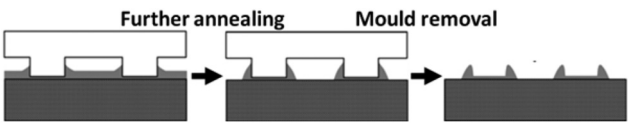

Fig. 2 Schematic representation of the effect of extended annealing. Adapted from ref. 19. Copyright with permission from the American Chemical Society (2014).

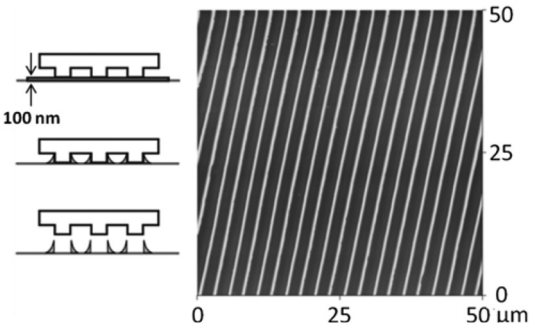

Fig. 3 A schematic illustration of CFL applied on thin polymer films and an AFM micrograph of the obtained polymer pattern. Adapted from ref. 20. Copyright with permission from the American Chemical Society (2014).

methodology with which to fabricate downsized pattern features.

2.4. Miscellaneous aspects

The molecular weight (or viscosity) of the polymer also has a direct impact on CFL. It is not hard to imagine that polymers with low or high viscosities will behave differently during CFL within the experimental time scale. If the polymer is too mobile, the system immediately dewets but if the polymer is too viscous, it does not reach the optimal pattern geometry. The viscosity data of the polymer have been related to the quality of the pattern in CFL.[22] The dynamics of polymers in thin films, however, are different from those in the bulk phase. Hence comprehensive studies are still needed to understand the relationship between the dynamics of the polymer in thin films and the process of CFL and the final morphology of the polymeric pattern.

As mentioned in section 2.3, polymers within the voids of a mould undergo a dewetting process which causes the morphological change of the pattern. The extent of this change is highly dependent on the processing time, as well as the temperature. Though it is not easy to predetermine the morphology of the final patterned structure, one can work out the correlations between the pattern morphology and the parameters (*i.e.* aspect ratio of the mould, thickness, molecular weight of the polymer, process time and temperature) within a specific experimental setup. Furthermore, this was demonstrated experimentally by Korczagin *et al.*[22] where copolymers consisting of ethylmethylsilaferrocenophane and dimethylsilaferrocenophane with different molecular weights underwent CFL under the same conditions. Patterns of the lowest molecular weight polymer coalesced into droplets due to dewetting while films of the highest molecular weight polymer produced incompletely developed lines. Patterns of the mid molecular weight, however, were well developed, demonstrating the importance of balancing each aspect of the polymer processing conditions.

2.5. Limitations

Though elastomeric behaviour is required for conformal contact between the stamp and the substrate, it is a potential source of problems in certain designs. If the aspect ratio of the stamp is too high, stresses originating from gravity, adhesion or capillary forces may result in lateral collapse of relief structures. In addition, if the aspect ratio is too small, the recessed region will not be able to maintain its structure during stamping.[23] These problems pose resolution limits on the CFL process, making the fabrication of high density and aspect ratio sub-100 nm structures a challenge with conventional elastomeric moulds.[24] However, derivatives of CFL have been developed to overcome these limitations and they are further discussed in this review.

3. Recent developments in CFL methods

3.1. Two-step CFL

Two-step CFL has brought more versatility into this new lithography technique.[11,25,26] Suh *et al.* demonstrated this by first placing a mould on the surface of a polystyrene layer which was spin-coated onto a silicon wafer substrate, followed by the annealing of the whole set at 150 °C for 1 h resulting in a polymer structure as shown in Fig. 4a.[26] After the first mould was removed, the second mould was placed on the patterned polystyrene film and orientated at 90° to the underlying pattern. The sample was then heated in an oven for the second time at various annealing times. Fig. 4b shows the morphological evolution of the polymer microstructures formed as a function of annealing time when the second mould was used. In the initial stage, the underlying polymer selectively wets the second mould walls, where the polymer and mould are in contact, leading to the formation of a polymer meniscus within the void space. As the polymer continuously fills up the void of the second mould, the mass underneath the mould becomes depleted, leading to the lowering of the mould and eventually leading to the contact of the mould with the substrate. A second meniscus begins to form when the mould comes in contact with the substrate. In the final stage, the first meniscus reaches the ceiling of the second mould and becomes flat, while the lowest part of the second meniscus continues to rise until the formation of regularly spaced holes which are located at the centre of the final polymer stripe (after 60 min and 90 min annealing). If the annealing time is increased to 3 h, the holes become completely filled. The width and height of the mould largely affect the evolution of the final pattern.

With the assistance of UV irradiation, two-step CFL can fabricate monolithic micro/nanoscale structures on a UV curable polymer such as PUA (polyurethane acrylate).[11,27,28] Fig. 5 illustrates the process of this two-step UV-assisted CFL. In order to successfully apply the second lithographic step on the microstructure generated by the first, the UV-curable PUA

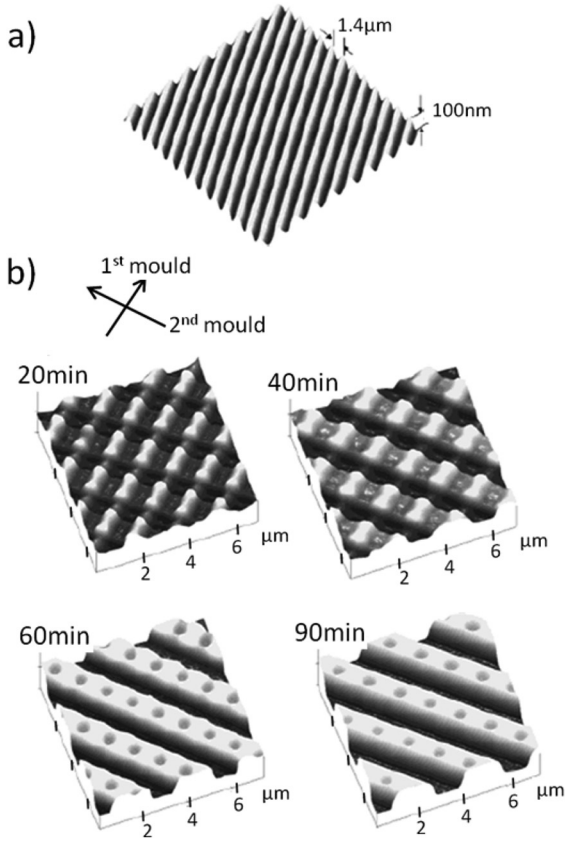

Fig. 4 (a) A three-dimensional view of the patterns after the first CFL step. (b) Transient microstructures as a function of annealing time (20, 40, 60 and 90 min). The second mould was orientated at 90° with respect to the pattern direction of the underlying structure. The height scale is 300 nm and the width is 8 μm. Adapted from ref. 26. Copyright with permission from John Wiley and Sons (2014).

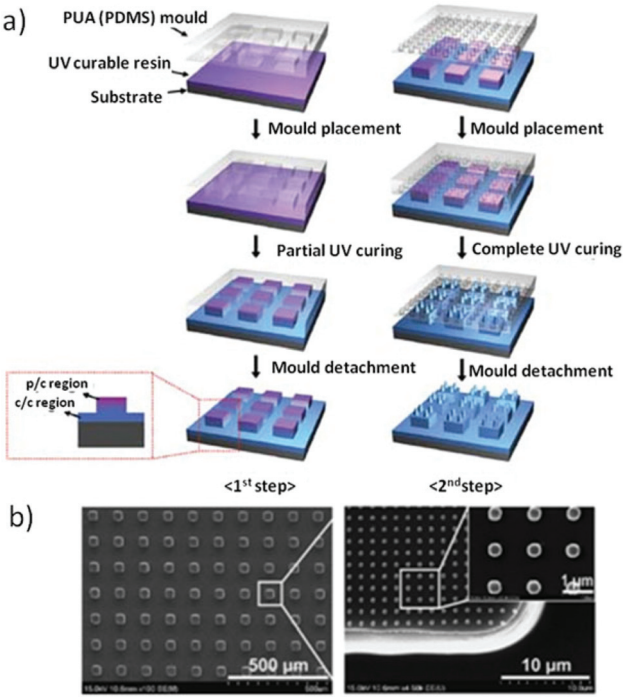

Fig. 5 (a) A schematic illustration of the two-step UV-assisted CFL (p/c: partially cured, c/c: completely cured). (b) SEM images of dual scale hierarchical structures. For microstructures, 40 μm boxes with 80 μm spacing and 40 μm height were fabricated (left) and a high resolution image showing the structure with 400 nm dots (800 nm spacing, 500 nm height). Adapted from ref. 11. Copyright with permission from John Wiley and Sons (2014).

resin is used and partially cured by exposure to UV light. The trapped or permeated air inside the mould inhibits radical polymerization of the PUA resin, rendering the top layer partially cured. The UV-irradiation time for the partial curing of the microstructure is a crucial parameter. If the curing time is too short, the microstructures collapse easily. However, if PUA is over irradiated, it becomes too hard to be patterned in the second step. Hence, patterning nanostructures over preformed microstructures *via* CFL is only possible when a suitable curing time, which allows the top section to remain fluidic, is applied.

Similarly, Shi *et al.* have also demonstrated the feasibility of fabricating these micro/nanoscale hierarchal structures onto poly-methyl methacrylate (PMMA) by combining hot embossing and CFL.[29] An initial microscale pattern is imprinted with an Obducat imprinter. Following a specified embossing time, the substrate is cooled and the polymer is demoulded. The second imprinting process is then carried out by placing a PDMS mould, with lattice spacings of 3–5 μm, onto the preformed microstructure. CFL was then carried out, resulting in nanostructures forming on the microstructure pattern. By making adjustments to the pressure, temperature and time at which CFL is carried out, the resulting nanostructures could be tailored. Importantly, annealing at lower temperatures tended to result in nanostructures with lower structure heights. This was attributed to lower temperatures restricting the movement of the polymer chains in the mould cavity and hence producing a polymer melt with higher viscosity.

3.2. Pressure-assisted CFL

The deformation of conventional elastomeric moulds such as PDMS has been reported as a hindrance in fabricating sub-100 nm high-density and high-aspect-ratio patterns *via* CFL. To overcome this, Khang *et al.* introduced the concept of pressure-assisted CFL (PA-CFL) where a hard, permeable fluoropolymer mould is used in preference to an elastomeric mould.[24] The use of a stiff, permeable mould not only overcomes mould deformation but also negates the limiting effect compressed air (between the mould and the substrate) has on capillary action. Hence, in principle, no resolution limitation should be observed. Furthermore, due to the low surface energy and its inert nature, the fluoropolymer mould can be cleanly removed from the patterned polymer without any mould surface treatment and without surface deterioration over multiple patterning steps. In combination with the stiff fluoropolymer, a slight pressure (~2–3 bar) is applied to achieve a conformal contact between the mould and the

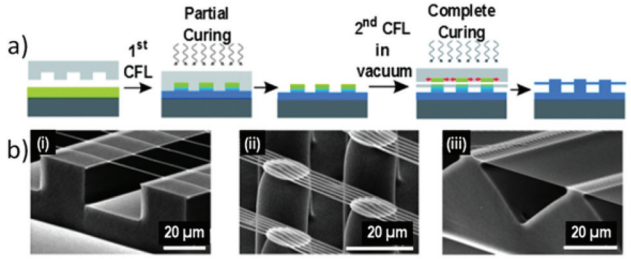

Fig. 6 (a) Schematic illustration of the fabrication of bridged hierarchical structures using a vacuum-assisted two-step CFL and (b) SEM images of various monolithic nanowire bridge structures formed over each underlying microstructure. Adapted from ref. 27. Copyright with permission from the Royal Society of Chemistry (2014).

polymer layer to be patterned. The resulting structures from this study varied from regular square patterns (1 μm × 2 μm), dense lines (80 nm line-width) and meandering lines and dots (250 nm wide).

The elastic deformation of PDMS has also been intentionally employed to overcome the unexpected dewetting process. A constant external pressure (~4 bar) exerted at the interface between the mould and the thin polymer film can push the contacting polymer into the void space, resulting in a residue-free patterning.[30]

3.3. Vacuum assisted CFL

In the two-step UV-assisted CFL, partial curing of the UV-curable polymer has been utilized to create multi-scale hierarchical structures. A partially cured PUA polymer, however, is less fluidic and not able to move over a long channel. This can be overcome under low vacuum pressures ($\approx 10^{-2}$ Pa) where changes in the pressure drive the PUA polymer into filling up long channels even in a nano-scale mould.[31] This is demonstrated in Fig. 6a which illustrates the partially cured upper layer filling into the channel of the mould by an omni-directional hydraulic pressure gradient. The SEM images of the resulting suspended bridge structures are shown in Fig. 6.

3.4. Solvent-assisted CFL

Solvent assisted CFL uses a solvent instead of temperature to soften the material. Cross-linked PDMS swells in a number of solvents but still retains good mechanical strength. Due to this swelling, a PDMS mould can act as a solvent container. When a swollen PDMS mould is placed on the polymer thin film surface, the solvent within the PDMS mould will diffuse onto the polymer film under slight pressure. The thin polymer film in contact with the PDMS mould can then be dissolved in or swell upon contact with the solvent to become mobile. The dissolved polymer is squeezed out from the areas of contact, filling the voids of the mould due to capillary forces. When the PDMS mould is lifted up, patterning of a thin polymer film is realized.[32]

Though solvent assisted CFL does not comply with the original definition of CFL which utilizes the combination of capillary forces with a polymer melt at high temperatures ($T > T_g$),

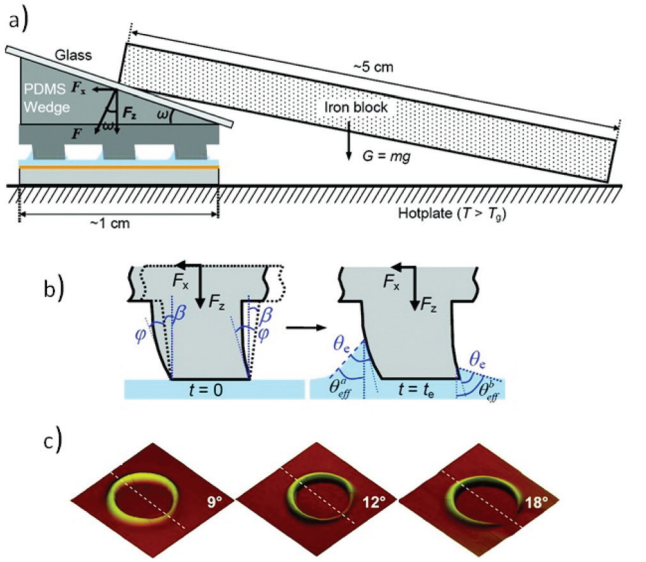

Fig. 7 (a) Schematic illustration of a deflected CFL setup. (b) Schematic illustration of the deformed pillars of a PDMS mould and the capillary rise of the polymer melt during deflected CFL. (c) 3D AFM (5 μm × 5 μm) images of asymmetric polymer rings generated under different forces ($F \approx 330$, 449 and 624 nN on each PDMS pillar). Adapted from ref. 33. Copyright with permission from the American Chemical Society (2014).

we would, however, like to review it as an extension of CFL as it is a method which points out a new pathway where CFL can be applied at low temperatures.

3.5. Deflected CFL

Recently, a novel variation of CFL to generate asymmetric polymeric ring structures by applying external forces to a PDMS mould has been reported.[33] The mechanism for the formation of asymmetric rings is caused by the deflection of cylindrical pillars protruding from the PDMS mould. A typical deflected CFL is carried out by placing a PDMS wedge with an angle, ω, on the PDMS mould. Following this, an iron block is placed on the PDMS wedge to introduce an external force, F (Fig. 7a). F can be resolved into F_x, the force horizontal to the substrate, and F_z, the force vertical to the substrate. An external force causes the deformation of the PDMS mould upon contact with the polymer layer, which leads to an asymmetric capillary rise (Fig. 7b). Fig. 7c shows an example of the resulting asymmetric polymer ring pattern generated from the deflected CFL. Asymmetric structures based upon triangular and square-shaped pillars can also be fabricated. The asymmetric polymeric rings can be readily transferred to an underlying gold layer to generate split ring structures with tunable opening angles. This method of transferring the pattern from the polymeric pattern to the substrate will be described in section 4.2.

3.6. Alternative moulding resins

Despite the extensive use as an elastomeric moulding material in soft lithography, the low modulus (1–10 MPa) of PDMS elastomers, coupled with high viscosity precursors, makes it difficult to fabricate moulds with sub-20 nm patterns. These 2

properties can potentially lead to the incomplete filling of master mould cavities and result in mould failure during removal.

As an alternative to PDMS, Zheng *et al.* have developed a silicon derivative known as "D_4^H/D_4^V",[34] with several advantages over PDMS while maintaining some key aspects. For example, its UV transparency still allows for UV assisted CFL, however its low viscosity and high modulus allow for the printing of small scale features and lithography at high pressures respectively. Consisting of closely linked silicones, D_4^H/D_4^V is prepared by a platinum catalysed reaction between tetramethylcyclotetrasiloxane and tetramethyltetravinylcyclotetrasiloxane. Using commercial blu-ray discs and electropolished aluminium as masters, sub-40 nm structures were fabricated *via* CFL. In assessing the replication performance of the moulds, 2 "granddaughter" structures were fabricated with no apparent damage or change in morphology.

4. Pattern transfer

4.1. Patterned binary polymer brushes

Patterned polymer-grafted layers, known as "brushes", have drawn significant attention because of the diversity of chemical structures suitable for brush formation and the physical/mechanical robustness of the grafted films. CFL can expose the surface of the underlying substrate, producing a pattern with two different surface properties. This nature of CFL makes it suitable for patterning binary polymer brushes.[12,35,36] The patterned polymer can become one constitution of the final pattern or be used as a mask to facilitate a selective polymer grafting process.

An example shown in Fig. 8 is based on the use of a PS mask to prevent grafting on the fraction of a surface protected by the polymer pattern. A thin layer of an epoxy polymer is first deposited on the surface of a silicon wafer for the initial surface modification. A macroinitiator, of atom transfer radical polymerization (ATRP), is then synthesized on the substrate surface by a reaction between epoxy groups of the polymer and the carboxy functionality of a halogen-containing carboxylic acid. Following this, an ultrathin PS film is deposited to cover the primary initiating layer. CFL is conducted and the PDMS mould was peeled off after cooling down to room temperature. CFL results in the generation of patterned PS (Fig. 8b). Consequently, part of the macroinitiator layer becomes exposed and available for brush synthesis, whereas other parts remain covered with PS and are thereby protected from the grafting of polymer chains. Surface-initiated ATRP was then conducted, and the first polymer brush was anchored to the uncovered fraction of the surface. After the grafting is complete, the PS mask is removed and the second brush was synthesized on the areas previously protected. This succession of procedures leads to the generation of a binary patterned polymer brush (Fig. 8c).

Although the first surface initiated polymerization (SIP) must be conducted in an environment that does not dissolve

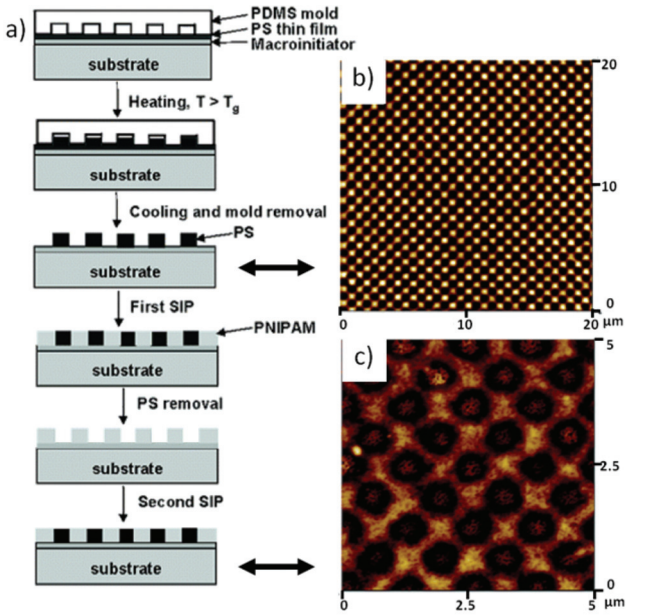

Fig. 8 (a) Schematic illustration of patterned surfaces created by CFL and surface-initiated polymerisation. (b) AFM topography image of a PS pattern (20 × 20 μm). (c) AFM topography image of binary polymer patterned brushes of poly(PEGMeMA) and PNIPAM (5 × 5 μm). Adapted from ref. 12. Copyright with permission from the American Chemical Society (2014).

the mask that is introducing the pattern, there are no specific restrictions for the second SIP. Virtually any polymer/copolymer obtainable by the ATRP method can be anchored to the surface at this stage of the process. Therefore, a variety of interesting combinations of binary patterned polymer brushes can be attained *via* CFL.

4.2. Transfer of patterns to the substrate

Polymeric patterns created by CFL can be further transferred to an underlying substrate by the assistance of selective etching techniques, such as reactive ion etching, wet-chemical etching, and Ar^+ ion milling.[20,37–41] An example is shown in Fig. 9, where a PS pattern is used as a mask to transfer a pattern to a gold substrate *via* reactive ion etching and Ar^+ ion milling.

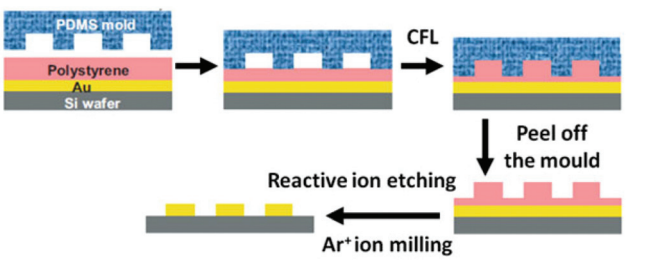

Fig. 9 Schematic of the generation of gold patterns on a silica wafer. Adapted from ref. 37. Copyright with permission from John Wiley and Sons (2014).

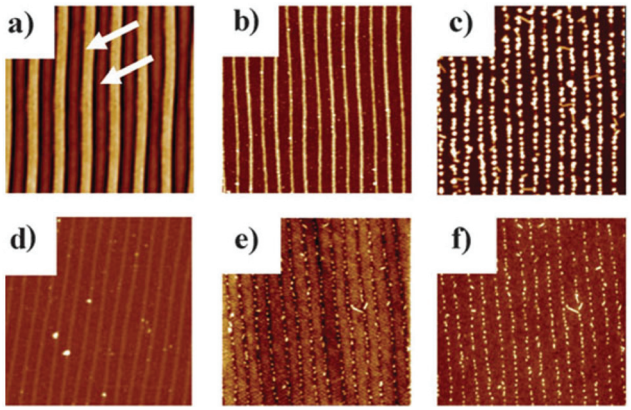

Fig. 10 AFM images of (a) PS pattern on a PGMA surface obtained by CFL, (b) PVP stripes obtained *via* solvent-assisted grafting, (c) Ag NPs adsorbed onto PVP patterns, (d) PVP stripes after transferring Ag NPs onto the PDMS matrix. (e) Topography and (f) phase images of Ag NPs embedded onto the PDMS matrix (5 × 5 μm). Adapted from ref. 42. Copyright with permission from the Royal Society of Chemistry (2014).

4.3. Alignment of nanoparticles

Ag nanoparticles assembled on patterns of the mould can be transferred onto freestanding transparent polymer films by CFL.[42] The general procedure for creating Ag NP one dimensional arrays consists of several steps. First, a thin layer of PGMA (poly(glycidyl methacrylate)), which contains epoxy functionalities, is deposited onto the surface of a silicon wafer. Next, a thin PS film is deposited by dip coating to cover the PGMA layer. A PDMS mould with the pattern of interest is placed over the PS film to conduct CFL which results in a patterned PS film (Fig. 10a). The key aspect of this step is that the PS material acts as a resist protecting part of the reactive PGMA surface. Consequently, the unprotected part of the reactive layer is exposed and available for solvent-assisted grafting the carboxy-terminated PVP chains at 40 °C. After grafting is completed, the PS mask is removed with a solvent, leaving the patterned PVP brush on the surface (Fig. 10b). Polyvinylpyrrolidone (PVP) has good affinity to silver, hence the patterned PVP surface is able to assemble Ag nanoparticles (50–70 nm in size) onto an array of one-dimensional chain-like structures (Fig. 10c). The nanoparticle structures can be transferred completely onto a PDMS freestanding film by a simple cure and peel-off procedure (Fig. 10d–f).[43]

The approach of using a resist can also be used to fabricate nanoparticle arrays on layer-by-layer (LBL) films.[44,45] LBL assembly is an effective and versatile technique to fabricate thin multilayer films.[46] Though selective attachment of functional materials on these films has been demonstrated, achieving this over large areas has been a challenge as strict control of the surface morphology and pH or ionic strength of solution is required. By capillary transfer lithography, a derivative of CFL, Tsukruk *et al.*[44,45] have demonstrated the feasibility of using this approach to deposit PS and poly(allylamine hydrochloride) (PAH) based sacrificial resists to form encapsulated arrays of carbon nanotubes and gold nanoparticles within LBL films.

Similarly, this approach can be adapted to fabricate crossbars of nanowires.[47] Utilising a double step micropatterning of PS resists, silver nanowire arrays can be drop cast perpendicular to each other to form pairs of L and T shapes as well as crossbars.

4.4. Proteins, viruses and cell patterning

Exposing substrates during CFL will create two distinctly different regions which can be pretreated or further modified with different functionalities. This potentially allows proteins, viruses, and cells to preferentially bind to specific regions of a patterned surface. Applying CFL on a thin uniform PEG-based (poly(ethylene glycol)) film results in patterned structures which consist of two regions: the moulded PEG surface and the exposed substrate surface. The patterned PEG structure acts as a physical and biological barrier for the adhesion of proteins and cells ensuring that site-specific adsorption can only occur on the exposed substrate area.[48,49] Subsequently, this can allow for the fabrication of viral arrays whereby viruses can adhere to specific regions of a pattern based on their binding affinity for the PEG surface.[50]

5. Applications of CFL

Although CFL was initially developed as a technique to pattern polymer films, its versatility has led to various wide ranging and diverse applications.

5.1. Fabrications of second-generation polymer moulds

Combining CFL with other techniques such as replica moulding, nanoimprint lithography, wet etching, and μ-contact printing allows for the fabrication of high-resolution (~100 nm), second-generation moulds for soft lithography.[39,51,52]

Fig. 11 depicts a schematic representation of CFL, in combination with replica moulding, to generate submicrometer-sized features in thin gold layers on silica. First, a PDMS mould is fabricated from a master. The PDMS mould is then placed on a thin layer of PMMA. As the thin layer of PMMA is insufficient to fill up the whole void between the mould and the substrate, it forms a meniscus along the protruding end of the PDMS mould during CFL. The resulting submicrometer-sized PMMA pattern can function as a high-resolution second-generation master for generating a second-generation PDMS mould. Multiple copies of the PDMS mould can be achieved without noticeable degradation or damage of the PMMA master. μCP (microcontact printing) of octadecanethiol (ODT) on a 20 nm thick gold layer and subsequent selective wet chemical etching of the gold result in the fabrication of trenches in the gold layers (Fig. 11e). Alternatively, one can microcontact print with PTMP (pentaerythritol-tetrakis(3-mercaptopropionate)) and protect the bare gold by dipping in ODT solution. Selective wet chemical etching of the area of gold with PTMP on the top results in gold lines (Fig. 11g). The

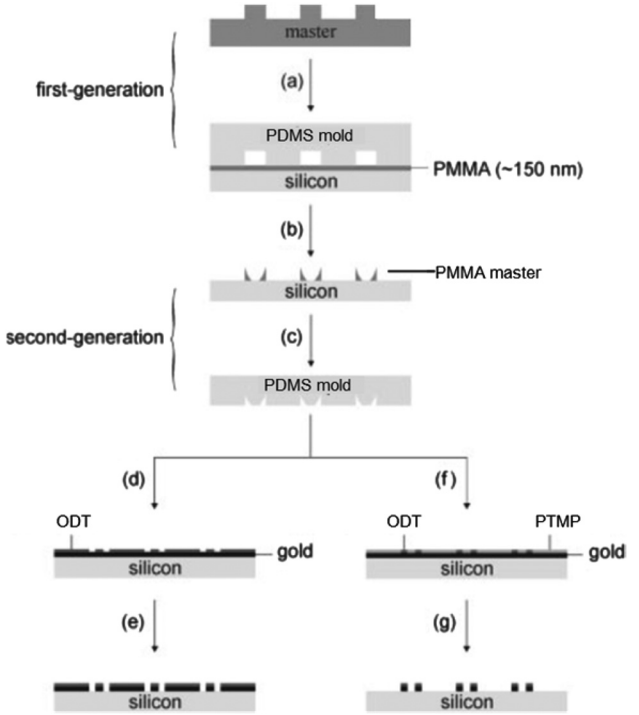

Fig. 11 Schematic representation of the fabrication of second-generation PDMS moulds by CFL and replica moulding. (a) The PDMS mould is fabricated from a master by replica moulding. (b) CFL is carried out on thin PMMA layers to fabricate second-generation PMMA masters. (c) A second-generation PDMS mould is fabricated from the PMMA master by replica moulding. (d)–(g) μCP (microcontact printing) followed by selective wet chemical etching of the gold results in traces of gold (e) and gold lines (g). Adapted from ref. 39. Copyright with permission from John Wiley and Sons (2014).

major advantage of this method over existing traditional mould fabrication is the simplicity of CFL, where no cleanroom facilities are required.

5.2. Engineering biomimetic hierarchal structures

Functional surfaces in nature often have multi-scale hierarchical structures. Two well-known examples are the lotus leaf and hairs on gecko feet. The initial experiments to fabricate biomimetic structures *via* CFL were carried out by Jeong *et al.*[53] By controlling the capillarity and surface adhesive forces during the mould removal process, high aspect ratio (aspect ratio >20) PMMA nanohairs were fabricated in a single step. The mould removal process not only produces the stretched nanohair structure but also results in bulges at the tip of each hair which are larger than the rest of the nanohair structure. This concept was further developed by fabricating such structures *via* two-step CFL.

Two-step CFL has shown great potential as a tool to mimic nature's multi-scale functional surfaces. Partial UV curing in the first CFL step with a micro mould allows for the second mould, with nanoscale features, to be patterned over the top, resulting in the formation of a monolithic, hierarchical structure (Fig. 12a). By choosing angled nanostructures with high-aspect-ratios as the second mould, spatula-like, slanted nanohairs on setae-like microhairs (patterned by the first CFL step) can be generated, as shown in Fig. 12a and b.[54] The size of the microhairs (diameter of 5 μm and height of 25 μm) is selected by considering the actual size of gecko's setae (diameter of 5 μm and height of 100 μm) (Fig. 12c). However, the height of the microstructures obtained is limited to 40 μm because of the structural instability caused by a relatively low elastic modulus of a soft PUA mould. One notable feature is that there is no interface between the micro- and nano-hairs, which is one advantage of the 2-step UV-assisted CFL. In addition, these monolithic, multiscale structures also demonstrate promising applications as dry adhesives. Similar to the system observed in gecko feet, it enables directional adhesion to occur without fouling by sticky materials after several repetitive cycles of attachment and detachment.

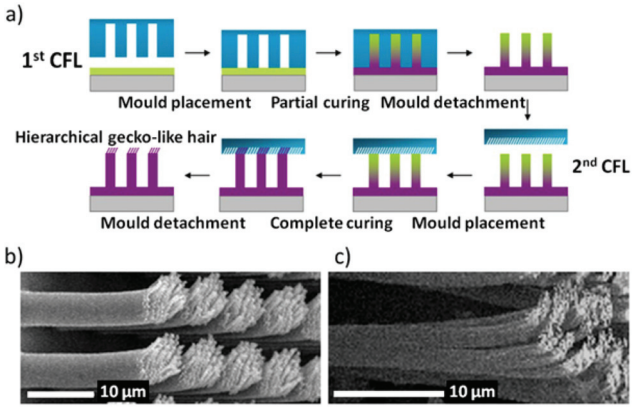

Fig. 12 (a) Schematic illustration of the fabrication of dual-scale hierarchical hairs by 2-step CFL. (b) A tilted SEM image of the hierarchical hairs obtained. (c) A tilted SEM image of real gecko foot hair, demonstrating similarity to the artificial hair shown in (b). Adapted from ref. 54. Copyright with permission from the National Academy of Sciences, USA (2014).

Though successful, the proposed methodology of fabricating structures, purely *via* CFL, was heavily reliant on the careful modulation of adhesive forces at the mould–substrate interface and the tuning of both the polymer viscosity and crosslinking density. To simplify this fabrication process, Zhang *et al.* developed an alternative robust methodology combining CFL and conventional photolithography to fabricate hierarchical micropillar arrays with variable aspect ratios.[55] By exploiting the thermoplastic and photosensitive nature of SU-8, a commercially available photoresist, micropillar arrays were initially fabricated *via* CFL. This was followed by photopatterning through a mask with a microdot array. To fabricate hierarchical structures from the imprinted film, 2 options were investigated: (i) immersing the film in isopropanol, resulting in bilevel dual scale patterns with micropillar arrays atop individual microposts and (ii) thermal reflowing of unexposed regions, effectively melting the unexposed micropillars and forming monolevel dual scale micropillar arrays.

5.3. Patterned surface for regulating cell growth

The effects of surface topography on cell behaviour have been studied for half century. Recent developments in lithographic and nanofabrication techniques have accelerated development in this area. Already, CFL has shown its potential application in regulating cell growth. Highly uniform PEG nano-pillars (Fig. 13a) fabricated by UV-assisted CFL have been used as cell culture platforms for primary rat cardiomyocytes. It was found that although cell adhesion substantially reduced compared to that on the glass control (a traditional substrate for cell growth), cell adhesion was significantly enhanced on PEG nano-pillars compared to those on the bare PEG controls. Furthermore, the PEG nano-pillars were found to stimulate adjacent cardiomyocytes into aggregating into colonies (Fig. 13b). These cardiomyocytes retained their conductive and contractile properties, as evidenced by observation of their beating in addition to their robust action potential generation. Despite this, several factors have to be taken into consideration when fabricating cellular substrates. For example, nanostructured PEG surfaces are hydrophobic compared to the bare PEG surface while its stiffness will decrease after patterning. These property changes may induce cardiomyocytes to behave differently.[56] Nevertheless, CFL has offered a simple way to control the cell–surface topography interaction. Hence, by fabricating patterns of varying densities and feature sizes, one can guide cell attachment, migration, and aggregation.[57]

In addition to controlling cell growth, similar nanotopographical features fabricated by CFL are able to influence the stem cell fate.[58–60] Linear arrays of 350 nm sized PUA nanogrooves have been reported to induce the differentiation of human embryonic stem cells (hESCs) into mature neurons after 5 days without differentiation into a glial lineage.[58] Though the mechanism of inducing differentiation was not reported, a similar study by Ahn *et al.* using human mesenchymal stem cells (hMSCs) reported that hMSCs respond to PUA nanoposts of varying densities by significantly regulating their cytoskeletal network stiffness.[59]

The ability to fabricate cell compatible substrates which aid the growth and differentiation of cells has led to the development of cell-material based therapeutics. Yang *et al.* have demonstrated the feasibility of such an approach.[61] Patterned PLGA substrates fabricated by CFL were found to induce the development and differentiation of primary muscle cells to form mature muscle patches. When transplanted into a Duchenne muscular dystrophy (DMD) mice model, a significant increase in the number of dystrophin-positive muscle fibers was observed, indicating possible dystrophin replacement and myogenesis *in vivo*. In contrast, these observations were not seen with flat muscle patches.

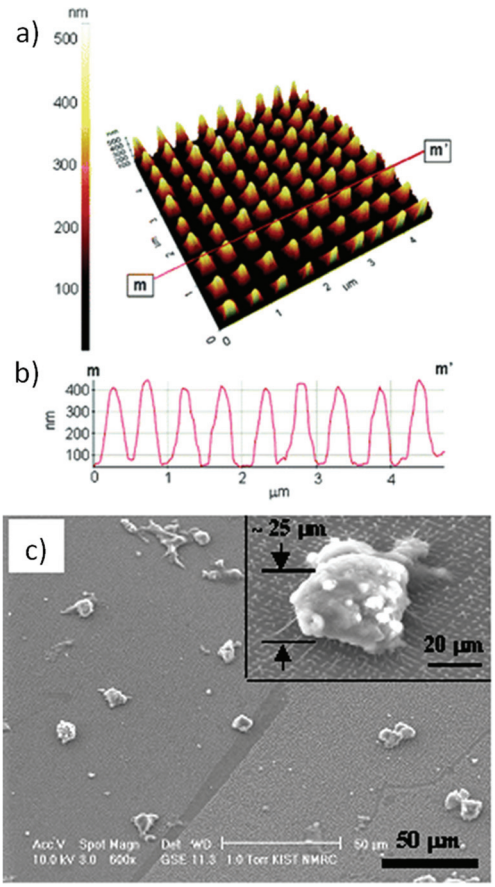

Fig. 13 (a) AFM image of height profile of PEG nano-pillars. (b) Cross-sectional analysis demonstrating uniform PEG nano-pillars with ~150 nm width and ~400 nm height. (c) Representative SEM images of aggregated cardiomyocytes cultured on the PEG nano-pillars. Adapted from ref. 56. Copyright with permission from the American Chemical Society (2014).

5.4. Engineering complex culture substrates

The ability to fabricate substrates with nanotopographies mimicking the ECM environment has enabled the study of fundamental cell biology questions without the use of animal models. Kahp-Yang Suh's group has developed *in vitro* wound healing tissue culture models to examine how fibroblasts respond to variable densities of micro and nanotopographies on a single substrate.[62,63] For example, while it was deemed that topography played a vital role in reorganising the process of ECM remodelling, the density of such topographical cues was an important aspect of the process. Similarly, Junsang Doh's group has used such complex tissue culture substrates to study the mechanisms of T cell migration on a variety of substrates ranging from linear grooves to zigzag structures mimicking complex tissue architecture and linearly aligned endothelial layers.[64–66] For a comprehensive overview of CFL applications toward cell and tissue engineering, one can refer to an early review paper from Suh's group.[67]

5.5. Confinement of proteins, viruses and cells

When a thin polymer film is subjected to CFL patterning, the substrate will be exposed after CFL. This selective exposure of the substrate creates two different surfaces with 2 different properties. If the exposed region is pretreated with an antibody against a specific virus along with an attachment resistant polymer, the resulting patterned surface can be used as spatial confinement for viruses.[13]

This selective immobilisation of biomolecules is also applicable to proteins. To date, Suh *et al.*[48] and Khademhosseini *et al.*[49] have demonstrated the feasibility of patterning both BSA and fibronectin with such a process. In addition, several groups have utilised CFL in conjunction with other novel techniques to fabricate protein patterns. For example, Kwon *et al.*[68] have used CFL with microscope projection photolithography (MPP) to fabricate multiscale protein pattern structures while Zemla *et al.*[69] have used inverted micro-contact printing to attach lentil lectin (LcH) onto 3D structures fabricated by CFL.

Similarly, if the patterned polymer film of interest is sufficiently thick, CFL can be used to generate microwell patterns of variable cell adhesivity. This enables the encapsulation of cell bodies and hence the formation of cellular patterns.[14,48,49,70] This approach was further extrapolated by layer-by-layer assembly of polyelectrolytes or ECM matrix proteins onto non-cell friendly regions, changing the surface biocompatibility. This enables the development of co-cultures where 2 cell types can be cultured on the same substrate in specific patterns.[71–74] This is beneficial in developing more realistic *in vitro* cell culture models where mimicking the multicellular nature of complex tissue *in vivo* is highly desired.[72,74]

5.6. Drug delivery platforms

In developing an alternative to delivering vaccines, Moga *et al.*[75] have utilised a process known as PRINT, to fabricate rapidly dissolvable microneedle patches for minimally invasive drug delivery. The scalable technique combines the "top down approach" of CFL with traditional polymerisation techniques to fabricate reproducible features on the micro- and nanoscale. Furthermore, the use of biodegradable and water soluble polymers in the fabrication process not only imparts water soluble properties but also allows for patches to be fabricated in less than 5 min. This is highly advantageous as it allows for both quick and affordable fabrication.

5.7. Engineering core–shell nanostructures

Hybrid core–shell nanostructures have a diverse range of applications in nanobionanotechnology,[76] optoelectrics[77] and energy research.[78] However, both the optical and electrical properties of such materials only function under specific constraints.[79,80] Current methods to fabricate these nanostructures have often resulted in irregular structures with wide size distributions. Hence, the major challenge in the field has been to develop a viable strategy for their fabrication. Hee-Tae Jung's group has developed CFL based approaches to fabricate hybrid Au core–shell nanostructures.[79,80] The use of CFL in their approach was highly favoured as it allowed for the simple and facile fabrication of highly periodic nanostructures with a narrow size range. For example, the plasmonic absorption of the nanostructures can be precisely tuned to a desired wavelength region by controlling factors such as the size or shape of the dielectric core and the metallic shell. Further constant interstructure spacing of the structures also results in enhanced absorption in the mid- and far-infrared spectral regions.[81] These criteria were achievable with CFL where the surface plasmon absorption could be tuned by changing the geometry of the PDMS stamp and fabrication conditions.[79]

5.8. Gas sensing

A "grafting to" approach in combination with CFL can be used to fabricate linear assemblies of Pd (palladium) nano-cubes through electrostatic interactions.[15] Pd nano-arrays with high density can be integrated into a circuit as a miniature hydrogen sensor. The typical procedure for fabricating Pd nano-arrays is illustrated in Fig. 14a. First, a silica wafer is modified with a reactive polymer containing epoxy functionalities, PGMA [poly(glycidylmethacrylate)]. The glycidyl methacrylate units of the PGMA chain not only serve to anchor the polymer to the silica substrate but the free groups also serve as reactive sites for the subsequent attachment of additional polymers with complementary functional groups. Following this, PS is dip-coated as the second layer. The PS layer here serves to provide as a chemical resist to selectively graft polymers onto the epoxy groups of PGMA following patterning. CFL in this instance results in the formation of alternating PGMA and PS stripes. Polyanionic PAA is then grafted onto PGMA. This allows positively charged Pd nano-cubes to electrostatically assemble onto the patterned surface. This can then be followed by washing steps to remove PS to obtain linear arrays of assembled Pd nano-cubes.

This is an example which demonstrates that by CFL in conjunction with a "grafting to" approach, it is possible to assemble nanomaterials into arrays as a platform for creating large area prints for developing sensors.

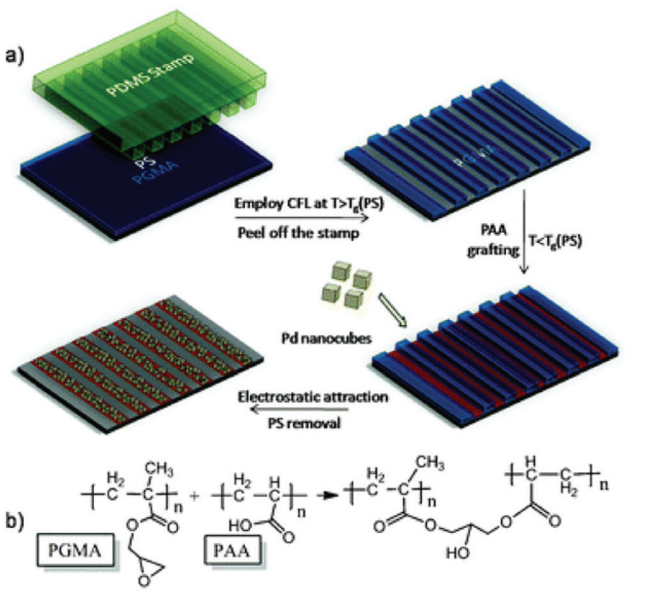

Fig. 14 (a) Schematic of patterning Pd nano-cube arrays by CFL in combination with a "grafting to" approach. (b) Chemical reaction of grafting PAA to PGMA. Adapted from ref. 15. Copyright with permission from the Royal Society of Chemistry (2014).

5.9. Solar cell technology

Recently, there has been much interest in developing more efficient solar cells in a cost effective and simple manner. Though several approaches such as utilising new narrow bandgap materials for photon harvesting or designing novel configuration cells have been reported, little attention has been paid to the problems involved in improving light trapping within solar cells.[82–84] While several groups have suggested the imprinting of nanostructures onto the active layer enhances light trapping,[85,86] current conventional imprinting techniques require samples to be removed from a nitrogen glove box and into an external environment where contact with oxygen and moisture leads to damage of the active layer. To overcome this, Cheng *et al.* have used CFL to fabricate nanosized gratings and nano-holes onto the surface of the ZnO and active layers of their solar cells.[87] Due to its simplicity, it was possible to imprint these nanostructures (*via* CFL) without removing the experimental setup from the nitrogen glove box, hence maintaining the integrity of the material. Furthermore, the imprinted structures resulted not only in enhanced light trapping as hypothesised but also the protrusion of the nanostructures into the active layer shortened the pathway for charge transfer, leading to an improved collection of charge and an increase in fill factor. Similar findings were published by other groups utilising CFL to improve the solar cell efficiency. Shir *et al.*[88] reported that SU8 epoxy nanostructures formed on monocrystalline silicon microcells *via* CFL not only improved the performance due to improved light trapping effects but also required less silicon to be used in the fabrication process. An *et al.*[89] reported significant improvements in solar cell efficiency, due to greater absorption and electrical enhancement, when CFL was used to pattern the microresonant cavity.

5.10. Optical devices

Citing its simplicity, the use of CFL in the manufacture of thin film transistor liquid crystal displays (TFT-LCD) has also been explored by Kim *et al.*[90] Currently, the use of a four colour pixel display (RGBW) is of great interest to manufacturers. As most of the light is absorbed by the colour filter the addition of a white sub-pixel enhances the efficiency of light transmission. Hence, every fourth pixel on an LCD substrate is devoid of material. When fabricating by conventional photolithography, an additional photo-masking step is required to fill up the void for surface planarisation prior to the addition of the column spacer. CFL, however, enables this process of planarisation to be carried out while simultaneously fabricating the column spacer and overcoat in a single step. Furthermore, in demonstrating its applicability in industry, the authors produced 2 different functioning TFT-LCD displays while utilising CFL as part of the manufacturing process.

This approach of patterning optically active materials *via* CFL was also used by Zhang *et al.*[91] Micro and nanoscale diffractive optical element (DOE) structures were fabricated onto a 3D concave lens over a short period of time while still maintaining the fidelity of the curved master mould. In comparison, this pattern fidelity is not attainable with decal transfer lithography, itself a modified soft lithography technique which uses planar elastomeric stamps to form patterns on curved surfaces.

5.11. Nanocrystal arrays

By fabricating templates with variable wettabilities *via* CFL, Suh *et al.* have demonstrated the feasibility such a technique has in not only guiding nucleation and growth but also forming ordered nanocrystal arrays.[92] Patterning the hydrophobic PEG copolymer onto hydrophilic glass or silicon dioxide creates 3D regions of alternating wettabilities. When briefly immersed in an aqueous solution of an organic salt, the solution selectively wets on the hydrophilic regions. As the solution eventually dries off, the salt crystals precipitate in the 3D microwells, forming nanocrystal arrays. Furthermore, adjustments in salt concentrations and microstructure sizes resulted in variable crystal sizes being attained. This approach was perceived to have several advantages. For example, the biocompatibility of the PEG copolymer would enable the technique to be applied to biological applications such as sensors and detectors.

5.12. Hydrogel patterning

Three-dimensional hydrogel patterns have been touted as viable alternatives to two-dimensional surfaces for biomedical applications. Due to the nature of such applications, the hydrogel material must satisfy key requirements including the ease of patterning, optical transparency and contain high densities of functional groups which allow for the incorporation of biomolecules. The favourable mechanical strength and compatibility with the CFL process have made PEG based hydrogels attractive materials in hydrogel patterning *via* CFL.[93–95] It must, however, be noted that in some instances, the use of a reactive polymer coating prior to the CFL process is required to stabilise the patterned hydrogel.[93] The purpose of such a coating is to simply act as an anchor to the surface substrate.

Patterned PEG-polyacrylamide beads (PEGA) have not only been demonstrated to induce cellular patterns but also the primary amine groups on the PEGA structures allow the structures to form a solid phase synthesis platform with which to attach various peptides for biological applications.[94] For example, short peptides with an *ortho*-aminobenzoic acid (Abz) group at the amino terminus and the 3-nitrotyrosine ($Tyr(NO_2)$) residue at the carboxyl terminus were synthesised onto the PEGA arrays/biochip to form a FRET based test for the presence of various proteases with distinctly different selectivities for amino acids flanking the cleaved amide bond.

6. Outlook

In the last ten years, CFL has developed into a versatile benchtop technique for large-area patterning. The applications of CFL are ever growing towards developing sensors, biomimetic

surfaces and self-assembled hierarchical systems. However, there are opportunities to extend this technique to several fields which have not yet explored this extensively. Phase separation of polymers on thin films is an attractive self-organizational process which might lead to a wide range of practical applications, such as fabricating polymer-based microelectronic circuits, antireflection coatings and polymer resists for lithographic semiconductor processing.[96–98] Very limited attempts have been made to CFL induced phase separation.[99] A closely related area which also has not been fully explored is the application of CFL on thin films of polymer blends.[100] Nature-inspired, multiscale hierarchical surfaces are of great research interest. Two-step CFL shows appealing characteristics in this field but only a few attempts have been demonstrated. There are also concerns that high temperatures ($T > T_g$) used in CFL are likely to degrade the electrical properties of semiconducting polymers. However, the versatility of CFL allows for low temperature patterning, a concept which needs to be further investigated. In summary, CFL is an important low cost, high throughput, large area patterning technique with enormous potential to make an impact as a mainstay lithography technique.

Conflict of interest

All authors declare no competing financial interests.

Acknowledgements

The authors would like to thank the Australian Research Council and the National Science Foundation (grant numbers DMR-1107786 and CMMI-0825773) for their funding support.

Notes and references

1 K. Y. Suh, Y. S. Kim and H. H. Lee, *Adv. Mater.*, 2001, **13**, 1386–1389.
2 T. Bhuvana and G. U. Kulkarni, *ACS Nano*, 2008, **2**, 457–462.
3 Y. Choi, S. Hong and L. P. Lee, *Nano Lett.*, 2009, **9**, 3726–3731.
4 H. Zhang, S.-W. Chung and C. A. Mirkin, *Nano Lett.*, 2002, **3**, 43–45.
5 H.-J. Jeon, K. H. Kim, Y.-K. Baek, D. W. Kim and H.-T. Jung, *Nano Lett.*, 2010, **10**, 3604–3610.
6 D. J. Lipomi, R. C. Chiechi, M. D. Dickey and G. M. Whitesides, *Nano Lett.*, 2008, **8**, 2100–2105.
7 J. W. Jeong, Y. H. Hur, H.-j. Kim, J. M. Kim, W. I. Park, M. J. Kim, B. J. Kim and Y. S. Jung, *ACS Nano*, 2013, **7**, 6747–6757.
8 J. W. Jeong, W. I. Park, L. M. Do, J. H. Park, T. H. Kim, G. Chae and Y. S. Jung, *Adv. Mater.*, 2012, **24**, 3526–3531.
9 X. Liao, K. A. Brown, A. L. Schmucker, G. Liu, S. He, W. Shim and C. A. Mirkin, *Nat. Commun.*, 2013, 4.
10 E. Kim, Y. Xia and G. M. Whitesides, *Nature*, 1995, **376**, 581–584.
11 H. E. Jeong, R. Kwak, J. K. Kim and K. Y. Suh, *Small*, 2008, **4**, 1913–1918.
12 Y. Liu, V. Klep and I. Luzinov, *J. Am. Chem. Soc.*, 2006, **128**, 8106–8107.
13 K. Y. Suh, A. Khademhosseini, S. Jon and R. Langer, *Nano Lett.*, 2006, **6**, 1196–1201.
14 J. M. Karp, J. Yeh, G. Eng, J. Fukuda, J. Blumling, K.-Y. Suh, J. Cheng, A. Mahdavi, J. Borenstein, R. Langer and A. Khademhosseini, *Lab Chip*, 2007, **7**, 786–794.
15 J. Zou, B. Zdyrko, I. Luzinov, C. L. Raston and K. Swaminathan Iyer, *Chem. Commun.*, 2012, **48**, 1033–1035.
16 P. S. Jo, A. Vailionis, Y. M. Park and A. Salleo, *Adv. Mater.*, 2012, **24**, 3269–3274.
17 K. Y. Suh and H. H. Lee, *Adv. Funct. Mater.*, 2002, **12**, 405–413.
18 K. Y. Suh, S. J. Choi, S. J. Baek, T. W. Kim and R. Langer, *Adv. Mater.*, 2005, **17**, 560–564.
19 H.-L. Zhang, D. G. Bucknall and A. Dupuis, *Nano Lett.*, 2004, **4**, 1513–1519.
20 I. Korczagin, S. Golze, M. A. Hempenius and G. J. Vancso, *Chem. Mater.*, 2003, **15**, 3663–3668.
21 K. Y. Suh, P. J. Yoo and H. H. Lee, *Macromolecules*, 2002, **35**, 4414–4418.
22 I. Korczagin, H. Xu, M. A. Hempenius and G. Julius Vancso, *Eur. Polym. J.*, 2008, **44**, 2523–2528.
23 D. Qin, Y. Xia and G. M. Whitesides, *Nat. Protoc.*, 2010, **5**, 491–502.
24 D. Y. Khang and H. H. Lee, *Adv. Mater.*, 2004, **16**, 176–179.
25 M. Park, D. C. Hyun, J. Kim, Y. S. Kim and U. Jeong, *Chem. Mater.*, 2010, **22**, 4166–4174.
26 K. Y. Suh and H. H. Lee, *Adv. Mater.*, 2002, **14**, 346–351.
27 H. E. Jeong, R. Kwak, A. Khademhosseini and K. Y. Suh, *Nanoscale*, 2009, **1**, 331–338.
28 H. E. Jeong, M. K. Kwak, C. I. Park and K. Y. Suh, *J. Colloid Interface Sci.*, 2009, **339**, 202–207.
29 G. Shi, N. Lu, H. Xu, Y. Wang, S. Shi, H. Li, Y. Li and L. Chi, *J. Colloid Interface Sci.*, 2012, **368**, 655–659.
30 H. Yoon, M. Kee Choi, K. Y. Suh and K. Char, *J. Colloid Interface Sci.*, 2010, **346**, 476–482.
31 R. Kwak, H. E. Jeong and K. Y. Suh, *Small*, 2009, **5**, 790–794.
32 X. Yu, Z. Wang, R. Xing, S. Luan and Y. Han, *Polymer*, 2005, **46**, 11099–11103.
33 Y. Cai, Z. Zhao, J. Chen, T. Yang and P. S. Cremer, *ACS Nano*, 2012, **6**, 1548–1556.
34 P. Zheng and T. J. McCarthy, *Langmuir*, 2011, **27**, 7976–7979.
35 B. Zdyrko, O. Hoy, M. K. Kinnan, G. Chumanov and I. Luzinov, *Soft Matter*, 2008, **4**, 2213–2219.
36 S. G. Im, K. W. Bong, B.-S. Kim, S. H. Baxamusa, P. T. Hammond, P. S. Doyle and K. K. Gleason, *J. Am. Chem. Soc.*, 2008, **130**, 14424–14425.

37 J. M. Jung, F. Stellacci and H. T. Jung, *Adv. Mater.*, 2007, **19**, 4392–4398.
38 S. Y. Lee, J.-R. Jeong, S.-H. Kim, S. Kim and S.-M. Yang, *Langmuir*, 2009, **25**, 12535–12540.
39 C. M. Bruinink, M. Peter, M. de Boer, L. Kuipers, J. Huskens and D. N. Reinhoudt, *Adv. Mater.*, 2004, **16**, 1086–1090.
40 S.-K. Lee, J.-M. Jung, J.-S. Lee and H.-T. Jung, *Langmuir*, 2010, **26**, 14359–14363.
41 S. Kim, J.-R. Jeong, S.-H. Kim, S.-C. Shin and S.-M. Yang, *J. Appl. Phys.*, 2006, **99**, 08G310.
42 B. Zdyrko, M. K. Kinnan, G. Chumanov and I. Luzinov, *Chem. Commun.*, 2008, 1284–1286.
43 S. Malynych, H. Robuck and G. Chumanov, *Nano Lett.*, 2001, **1**, 647–649.
44 C. Jiang, S. Markutsya, H. Shulha and V. V. Tsukruk, *Adv. Mater.*, 2005, **17**, 1669–1673.
45 H. Ko, C. Jiang and V. V. Tsukruk, *Chem. Mater.*, 2005, **17**, 5489–5497.
46 R. Gunawidjaja, C. Jiang, H. Ko and V. V. Tsukruk, *Adv. Mater.*, 2006, **18**, 2895–2899.
47 S. Chang, H. Ko, R. Gunawidjaja and V. V. Tsukruk, *J. Phys. Chem. C*, 2011, **115**, 4387–4394.
48 K. Y. Suh, J. Seong, A. Khademhosseini, P. E. Laibinis and R. Langer, *Biomaterials*, 2004, **25**, 557–563.
49 A. Khademhosseini, S. Jon, K. Y. Suh, T. N. T. Tran, G. Eng, J. Yeh, J. Seong and R. Langer, *Adv. Mater.*, 2003, **15**, 1995–2000.
50 P. J. Yoo, K. T. Nam, A. M. Belcher and P. T. Hammond, *Nano Lett.*, 2008, **8**, 1081–1089.
51 C. M. Bruinink, M. Péter, P. A. Maury, M. de Boer, L. Kuipers, J. Huskens and D. N. Reinhoudt, *Adv. Funct. Mater.*, 2006, **16**, 1555–1565.
52 X. Duan, Y. Zhao, A. Perl, E. Berenschot, D. N. Reinhoudt and J. Huskens, *Adv. Funct. Mater.*, 2010, **20**, 663–668.
53 H. E. Jeong, S. H. Lee, P. Kim and K. Y. Suh, *Nano Lett.*, 2006, **6**, 1508–1513.
54 H. E. Jeong, J.-K. Lee, H. N. Kim, S. H. Moon and K. Y. Suh, *Proc. Natl. Acad. Sci. U. S. A.*, 2009, **106**, 5639–5644.
55 Y. Zhang, C.-T. Lin and S. Yang, *Small*, 2010, **6**, 768–775.
56 D.-H. Kim, P. Kim, I. Song, J. M. Cha, S. H. Lee, B. Kim and K. Y. Suh, *Langmuir*, 2006, **22**, 5419–5426.
57 D. H. Kim, C. H. Seo, K. Han, K. W. Kwon, A. Levchenko and K. Y. Suh, *Adv. Funct. Mater.*, 2009, **19**, 1579–1586.
58 M. R. Lee, K. W. Kwon, H. Jung, H. N. Kim, K. Y. Suh, K. Kim and K.-S. Kim, *Biomaterials*, 2010, **31**, 4360–4366.
59 E. H. Ahn, Y. Kim, Kshitiz, S. S. An, J. Afzal, S. Lee, M. Kwak, K.-Y. Suh, D.-H. Kim and A. Levchenko, *Biomaterials*, 2014, **35**, 2401–2410.
60 K. Yang, K. Jung, E. Ko, J. Kim, K. I. Park, J. Kim and S.-W. Cho, *ACS Appl. Mater. Interfaces*, 2013, **5**, 10529–10540.
61 H. S. Yang, N. Ieronimakis, J. H. Tsui, H. N. Kim, K.-Y. Suh, M. Reyes and D.-H. Kim, *Biomaterials*, 2014, **35**, 1478–1486.
62 D.-H. Kim, K. Han, K. Gupta, K. W. Kwon, K.-Y. Suh and A. Levchenko, *Biomaterials*, 2009, **30**, 5433–5444.
63 H. N. Kim, Y. Hong, M. S. Kim, S. M. Kim and K.-Y. Suh, *Biomaterials*, 2012, **33**, 8782–8792.
64 K. W. Kwon, H. Park, K. H. Song, J.-C. Choi, H. Ahn, M. J. Park, K.-Y. Suh and J. Doh, *J. Immunol.*, 2012, **189**, 2266–2273.
65 K. H. Song, K. W. Kwon, S. Song, K.-Y. Suh and J. Doh, *Biomaterials*, 2012, **33**, 2007–2015.
66 K. W. Kwon, H. Park and J. Doh, *PLoS One*, 2013, **8**, e73960.
67 K.-Y. Suh, M. C. Park and P. Kim, *Adv. Funct. Mater.*, 2009, **19**, 2699–2712.
68 K. W. Kwon, J.-C. Choi, K.-Y. Suh and J. Doh, *Langmuir*, 2011, **27**, 3238–3243.
69 J. Zemla, A. Budkowski, J. Rysz, J. Raczkowska and M. Lekka, *Colloids Surf., B*, 2012, **90**, 144–151.
70 A. Khademhosseini, G. Eng, J. Yeh, J. Fukuda, J. Blumling, R. Langer and J. A. Burdick, *J. Biomed. Mater. Res., Part B*, 2006, **79A**, 522–532.
71 A. Khademhosseini, K. Y. Suh, J. M. Yang, G. Eng, J. Yeh, S. Levenberg and R. Langer, *Biomaterials*, 2004, **25**, 3583–3592.
72 J. Fukuda, A. Khademhosseini, J. Yeh, G. Eng, J. Cheng, O. C. Farokhzad and R. Langer, *Biomaterials*, 2006, **27**, 1479–1486.
73 S. Takahashi, H. Yamazoe, F. Sassa, H. Suzuki and J. Fukuda, *J. Biosci. Bioeng.*, 2009, **108**, 544–550.
74 J. Kim, H. N. Kim, K.-T. Lim, Y. Kim, S. Pandey, P. Garg, Y.-H. Choung, P.-H. Choung, K.-Y. Suh and J. H. Chung, *Biomaterials*, 2013, **34**, 7257–7268.
75 K. A. Moga, L. R. Bickford, R. D. Geil, S. S. Dunn, A. A. Pandya, Y. Wang, J. H. Fain, C. F. Archuleta, A. T. O'Neill and J. M. DeSimone, *Adv. Mater.*, 2013, **25**, 5060–5066.
76 B. D. Chithrani, A. A. Ghazani and W. C. W. Chan, *Nano Lett.*, 2006, **6**, 662–668.
77 X. Hu, J. Gong, L. Zhang and J. C. Yu, *Adv. Mater.*, 2008, **20**, 4845–4850.
78 Z. Peng and H. Yang, *Nano Today*, 2009, **4**, 143–164.
79 Y. K. Baek, S. M. Yoo, T. Kang, H. J. Jeon, K. Kim, J. S. Lee, S. Y. Lee, B. Kim and H. T. Jung, *Adv. Funct. Mater.*, 2010, **20**, 4273–4278.
80 J. S. Kim, H. J. Jeon, H. W. Yoo, Y. K. Baek, K. H. Kim, D. W. Kim and H. T. Jung, *Adv. Funct. Mater.*, 2014, **24**, 841–847.
81 S. Lal, N. K. Grady, J. Kundu, C. S. Levin, J. B. Lassiter and N. J. Halas, *Chem. Soc. Rev.*, 2008, **37**, 898–911.
82 C. Soci, I. W. Hwang, D. Moses, Z. Zhu, D. Waller, R. Gaudiana, C. J. Brabec and A. J. Heeger, *Adv. Funct. Mater.*, 2007, **17**, 632–636.
83 D. Zhao, L. Ke, Y. Li, S. Tan, A. Kyaw, H. Demir, X. Sun, D. Carroll, G. Lo and D. Kwong, *Sol. Energy Mater. Sol. Cells*, 2011, **95**, 921–926.

84 A. Wicklein, S. Ghosh, M. Sommer, F. Würthner and M. Thelakkat, *ACS Nano*, 2009, **3**, 1107–1114.
85 S.-I. Na, S.-S. Kim, S.-S. Kwon, J. Jo, J. Kim, T. Lee and D.-Y. Kim, *Appl. Phys. Lett.*, 2007, **91**, 173509.
86 C. F. Shih, K. T. Hung, J. W. Wu, C. Y. Hsiao and W. M. Li, *Appl. Phys. Lett.*, 2009, **94**, 143505.
87 Y.-S. Cheng and C. Gau, *Sol. Energy Mater. Sol. Cells*, 2014, **120**(Part B), 566–571.
88 D. Shir, J. Yoon, D. Chanda, J.-H. Ryu and J. A. Rogers, *Nano Lett.*, 2010, **10**, 3041–3046.
89 C. J. An, C. Cho, J. K. Choi, J. M. Park, M. L. Jin, J. Y. Lee and H. T. Jung, *Small*, 2014, **10**, 1278–1283.
90 J. Kim, T.-J. Song, J. H. Kim, S.-P. Cho, M. S. Yang, I.-B. Kang, Y. K. Hwang and I.-J. Chung, *Displays*, 2010, **31**, 82–86.
91 D. Zhang, W. Yu, T. Wang, Z. Lu and Q. Sun, *Opt. Express*, 2010, **18**, 15009–15016.
92 K. Y. Suh, A. Khademhosseini, G. Eng and R. Langer, *Langmuir*, 2004, **20**, 6080–6084.
93 K. Y. Suh, R. Langer and J. Lahann, *Adv. Mater.*, 2004, **16**, 1401–1405.
94 M. Zourob, J. E. Gough and R. V. Ulijn, *Adv. Mater.*, 2006, **18**, 655–659.
95 W.-S. Kim, M.-G. Kim, J.-H. Ahn, B.-S. Bae and C. B. Park, *Langmuir*, 2007, **23**, 4732–4736.
96 M. Böltau, S. Walheim, J. Mlynek, G. Krausch and U. Steiner, *Nature*, 1998, **391**, 877–879.
97 R. F. Service, *Science*, 1997, **278**, 383–384.
98 S. Walheim, E. Schäffer, J. Mlynek and U. Steiner, *Science*, 1999, **283**, 520–522.
99 X. Li, Z. Wang, L. Cui, R. Xing, Y. Han and L. An, *Surf. Sci.*, 2004, **571**, 12–20.
100 P. J. Yoo, K. Y. Suh and H. H. Lee, *Macromolecules*, 2002, **35**, 3205–3212.